Available online at www.sciencedirect.com
ScienceDirect
Journal of Power Sources 161 (2006) 1126–1132
JOURNAL OF POWER SOURCES
www.elsevier.com/locate/jpowsour

Effect of open circuit voltage on performance and degradation of high temperature PBI–H_3PO_4 fuel cells

Zhigang Qi *, Steve Buelte

Plug Power Inc., 968 Albany Shaker Road, Latham, NY 12110, USA

Received 27 April 2006; received in revised form 3 June 2006; accepted 6 June 2006
Available online 24 July 2006

Abstract

The impact of open circuit voltage (OCV) on the performance and degradation of polybenzimidazole–phosphoric acid (PBI–H_3PO_4) fuel cells operated at 180 °C was investigated. The OCV showed an initial quick increase in the first few minutes, followed by a much slower increase, and peaked after about 35 min. It then started an exponential and monotonous decline. Along with the decline of OCV, the performance of the fuel cell also declined. Operating the fuel cell with a load of 0.2 A cm^{-2} could temporarily boost the OCV and the fuel cell performance, but it could not recover the lost performance permanently. Electrochemical impedance spectroscopy (EIS) indicated significant loss of catalyst activity and increase in mass transport resistance due to the relatively high potential at OCV. X-ray diffraction (XRD) measurement showed that the cathode Pt crystallite size increased by as much as 430% after a total of 244.5 h of exposure to OCV.

Keywords: Open circuit voltage; Fuel cell; Polybenzimidazole; PBI–phosphoric acid; Catalyst sintering; Carbon corrosion

1. Introduction

Operating a fuel cell at high temperatures provides several system design and operational advantages. First, it reduces the complexity of a fuel cell system and thus enables higher system reliability and reduced materials and system assembly costs. For example, for a PBI–H_3PO_4 fuel cell operated at 180 °C, which can tolerate about 10,000 ppm CO, the low temperature shift (LTS) reactor and the preferential oxidation unit (Prox), which are required for a lower temperature proton-exchange membrane fuel cell, can be eliminated. Second, a PBI–H_3PO_4 fuel cell does not need aggressive humidification of the reactants, so there are few water management issues, and the humidifiers and related water pumps and manifolds required for lower temperature fuel cells are not needed. Third, high temperature fuel cells generate higher quality waste heat, so the size and the capacity of heat exchangers can be significantly reduced. The fuel cell's combined electrical and thermal efficiencies could be over 90%.

Conventional phosphoric acid (PA) fuel cells use silicon carbide (SiC) to host the phosphoric acid electrolyte. A lot of groundbreaking work was done at UTC fuel cells, and their work laid the foundation for the phosphoric acid fuel cells [1–4]. In early 1990s, Savinell and his research team at Case Western Reserve University started using PBI to host the phosphoric acid electrolyte [5–10]. PBI is an engineering material with good chemical/electrochemical stabilities and mechanical strength at high temperatures and in the presence of acids. The PA-doped PBI membranes were prepared by either imbibing a PBI membrane with PA or casting directly from a solution of PBI dissolved in a mixed acid solvent such as trifluoroacetic acid and PA. PA doping levels ranging from 3 to 16 mol of PA per PBI repeating unit were achieved. It was found that the mechanical properties of the membranes at high PA doping levels became poor and unsuitable for membrane-electrode assembly (MEA) fabrication. They suggested that the appropriate PA levels be between 3.5 and 7.5 mol of PA per repeating PBI unit.

More recently, Benicewicz and his research team at Rensselaer Polytechnic Institute (RPI) developed a sol–gel process to fabricate PBI–H_3PO_4 membranes [11–12]. This process is termed as the PPA process. The polymerization process to pro-

* Corresponding author. Tel.: +1 518 738 0229; fax: +1 518 782 7914.
E-mail address: zhigang_qi@plugpower.com (Z. Qi).

0378-7753/$ – see front matter © 2006 Elsevier B.V. All rights reserved.
doi:10.1016/j.jpowsour.2006.06.020

duce PBI was carried out using polyphosphoric acid (PPA) as both the polycondensation agent and the polymerization solvent, starting from materials such as tetraaminobiphenyl (TAB) and pyridine dicarboxylic acids. After polymerization, the PBI solution in PPA (PPA is a good solvent for PBI) was directly cast at 200–220 °C without separation or re-dissolution of the polymer. Upon casting, the hydrolysis of PPA to PA (PA is not a good solvent for PBI) by moisture absorbed from the surrounding environment induced a sol–gel transition that resulted in PA-doped PBI membranes. The resulting membranes displayed PA doping levels up to 25 mol of PA per repeating PBI unit, ionic conductivity as high as 0.2 S cm^{-1}, and stable mechanical properties at elevated temperatures.

PBI–H_3PO_4 fuel cells still face several key challenges. One challenge is the low performance due to the adsorption of phosphate anions onto the catalysts [2]. The adsorption blocks a significant portion of the catalyst sites, and thus the activation overpotential loss is quite high for both the reduction of oxygen at the cathode and the oxidation of hydrogen at the anode. Methods that can weaken the adsorption of phosphate anions should be able to effectively improve the fuel cell performance, but little progress has been made in this area so far.

Another challenge is the high corrosion rate of the amorphous carbon catalyst support such as Vulcan XC-72 [2,13]. Its corrosion can weaken the interaction between carbon supports and the catalyst particles, or even result in the complete detachment of the catalyst particles from the supports. This will in turn accelerate the agglomeration of catalyst particles and a reduction in the number of effective catalyst-H_3PO_4-reactant three-phase sites. Carbon corrosion/oxidation also causes the carbon surface to become more hydrophilic [14–16]. A highly hydrophilic surface will be more readily flooded by H_3PO_4, and result in higher mass transport resistance. The third challenge is the high dissolution and sintering rates of a catalyst such as Pt due to the high temperature [2,13,17–22]. Ferreira et al had a very thorough review on this topic [17]. Also, phosphate anions may be able to form complexes with Pt cations that could further accelerate the Pt dissolution process.

These challenges put more stringent demands on the fuel cell system operating algorithm. For example, during the lifetime of a fuel cell, it will experience both loaded and unloaded states. When power is required, the fuel cell is loaded to generate electricity. When power is not required, the fuel cell is not needed to generate electricity, and it is likely to be in an unloaded or no-load state. Without a load, the fuel cell will experience an open circuit voltage (OCV), which is close to 1 V per cell if there is fuel at the anode and air at the cathode, respectively. It is therefore necessary to figure out whether the OCV has any negative effect on cell performance and degradation, and how severe it is and how it changes with time if there is one. The result is then used to guide the design of the fuel cell system operating algorithm in order to achieve the highest stability and durability of the fuel cell system.

This article reports our investigation into the OCV effect on PBI–H_3PO_4 high temperature fuel cells operated at a cell temperature of 180 °C.

2. Experimental

2.1. Membrane-electrode assembly (MEA)

Experimental and proprietary MEAs with an active area of 45 cm^2 were obtained from suppliers. Vulcan XC-72 was used as the catalyst support, and the total Pt loading on anode/cathode was around 1.0 mg cm^{-2}. Carbon cloth-type materials were used as the catalyst layer backing. Each MEA was nicely packed in a sealed bag to prevent both exposures to air and adsorbing of water moisture. The bag was opened right before the cell assembly step, and the entire assembly process took no more than 10 min.

2.2. Open circuit tests

Single fuel cell tests were performed using a homemade 45 cm^2 active area test fixture. The test fixture was composed of a pair of graphite plates with serpentine flow-fields. Heating tapes were attached to the outside of both the anode and cathode end plates and the entire cell hardware was wrapped with thick insulating materials in order to warm up the cell quickly and to maintain its operating temperature.

Hydrogen and air at ambient pressure were used as the reactants at the anode and cathode, respectively. Unless otherwise stated, the cell temperature was controlled at 180 °C, and air entered the cell without any additional humidification, while hydrogen was humidified to a 52 °C dew point.

During the open circuit tests, the cell was kept at open circuit, and the OCV was recorded. The air flow rate was controlled at 1.35 times stoichiometric for a current density of 0.2 A cm^{-2}, while the hydrogen flow rate was about 0.5 SLM that was well over stoichiometric due to the use of a high flow mass flow controller. Periodically, fuel cell performance at current densities of 0.02, 0.2 A cm^{-2}, and the entire polarization curve were collected with constant air stoichiometry of 1.35 or 4.0.

2.3. Electrochemical impedance spectroscopy (EIS)

EIS was performed using a Hewlett Packard 6050 A system dc electronic load coupled with a Solartron SI 1250 frequency response analyzer. A perturbation of 50 mV was used during the measurement. A current density of 0.20 A cm^{-2} was applied to the fuel cell by the HP load bank, and the reactants flowed through both the anode and the cathode at the same stoichiometry as that used during normal fuel cell operation. In order to shorten the measurement process, each point at frequencies greater than 1000 Hz, between 1000 and 1 Hz, and less than 1 Hz was an average of 200, 10, and 2 measurements, respectively.

2.4. Cyclic voltammetry (CV)

An EG&G Potentiostat (model 273 A) was used to perform the cyclic voltammetry of the cathode at a cell temperature of 180 °C. During the measurement, the cathode was taken as a working electrode, and was supplied with nitrogen at a flow rate of 0.3 SLM; the anode was supplied with pure hydrogen at a

flow rate of 0.5 SLM and functioned as the counter and reference electrode. The potential was scanned between 0.05 and 0.50 V at 20 mV s^{-1}.

2.5. X-ray diffraction (XRD)

XRD measurement was performed using a Scintag X-ray diffractometer with a Cu (Kα) radiation source at 1.54 Å with a goniometer resolution of 0.02°. It uses a Peltier-cooled Si (Li) solid state detector, and can measure samples in the form of powders, thin films, or crystals. In this experiment, both the anode and the cathode were first peeled off of the membrane, and the anode and cathode samples were cut to a size of approximately 1 cm^2 before they were subjected to the XRD analyses separately. The samples were scanned at an angle range of 10–80°, with 0.03° of step size, and lasting 10 s at each step. After the scan was complete, the data were exported in .txt format and plotted using Microcal Origin Software. The peaks were fitted to calculate the full width at half maximum (FWHM) and the Debye–Scherrer equation was used to calculate the particle crystallite size.

3. Results and discussion

Fig. 1 shows the OCV change of a fuel cell during about a total of 350 h of testing (with 244.5 h at OCV). The OCV increased initially before it started an exponential and monotonic decline. The inset illustrates the OCV during its initial increase. The increase was quickest in the first few minutes, but showed down after about 5 min, and peaked after 37 min. For regions A and B (circled by dotted lines), the fuel cell was set at 0.2 A cm^{-2} for 7.5 and 96 h, respectively. In region A, the OCV did not show any apparent decline after the fuel cell was operated at 0.2 A cm^{-2} for 7.5 h (0.915 V versus 0.914 V). In region B, the OCV increased from 0.844 V (before setting the cell at 0.2 A cm^{-2}) to 0.875 after setting the cell at 0.2 A cm^{-2} for 4 h, and the OCV did not show apparent change during the 96 h at 0.2 A cm^{-2}. When the cell was returned to open circuit after 96 h

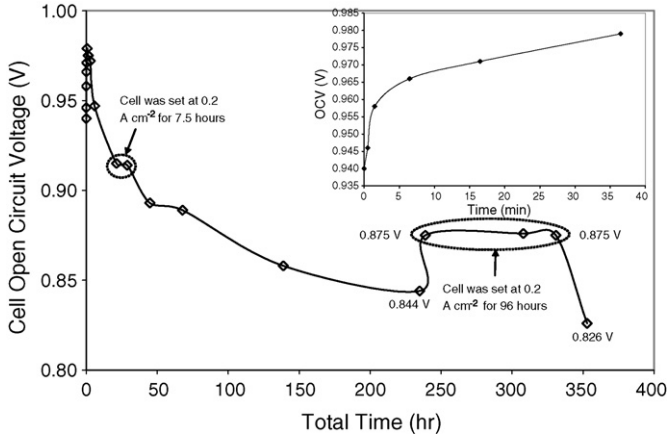

Fig. 1. OCV change with time when the cell was set at open circuit. The inset shows the OCV increase during the first 37 min. The fuel cell was operated at 0.2 A cm^{-2} for 7.5 and 96 h in the circled regions A and B, respectively.

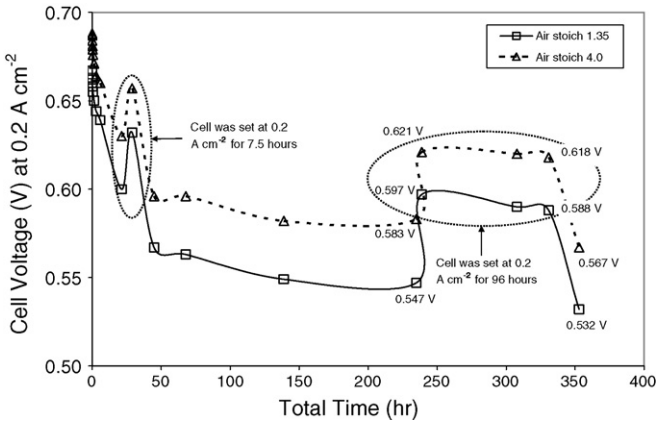

Fig. 2. Change of fuel cell voltage at 0.2 A cm^{-2} with time at open circuit with 1.35 (solid line) and 4.0 (dashed line) air stoichiometry, respectively. The fuel cell was operated at 0.2 A cm^{-2} for 7.5 and 96 h in the circled regions A and B, respectively.

at 0.2 A cm^{-2}, the OCV quickly declined from 0.875 to 0.826 V in 22 h, returning to the original OCV decline trend line. The OCV measurements shown in regions A and B were carried out by unloading the cell for about 1 min and then reloading it with a current density of 0.2 A cm^{-2}.

The fuel cell performance change during the 350 h of operation is shown in Fig. 2. The performance was periodically measured by momentarily interrupting the OCV test process with the application of a load for about 1 min. The higher and lower performance curves represent the results at air stoichiometry of 4.0 and 1.35, respectively. The trend of the curves is similar to the OCV curve shown in Fig. 1, except that the performance decline began immediately. The decline rate was fastest in the beginning of the OCV tests and most of decline occurred in the first 45 h.

When the cell was operated at 0.2 A cm^{-2} for 7.5 h in region A, the performance increased from 0.630 to 0.657 V and from 0.600 to 0.632 V at 4.0 and 1.35 times stoichiometric air flow, respectively. In region B, where the fuel cell was operated at 0.2 A cm^{-2} for 96 h, the performance initially increased from 0.583 to 0.621 V and from 0.547 to 0.597 V at 4.0 and 1.35 times stoichiometric air flow, respectively, in the first 4 h. During the remaining 92 h, the fuel cell performance declined slightly (3–9 mV). When the fuel cell was set at open circuit again, the performance quickly declined from 0.618 and 0.588 V to 0.567 and 0.532 V at 4.0 and 1.35 times stoichiometric air flow, respectively.

Clearly, setting a fuel cell at open circuit had significantly negative impact on its OCV and performance. Although operating the cell with a load of 0.2 A cm^{-2} did temporarily boost the OCV and the performance, it did not seem to have any permanent effect because the OCV and the performance returned to their decline trend lines once the cell was set at open circuit again. However, running a cell with a load of 0.2 A cm^{-2} did not cause any apparent OCV loss, and the performance only declined slightly.

Figs. 1 and 2 indicate that both the OCV itself and the fuel cell performance at 0.2 A cm^{-2} declined the most in the first 45 h

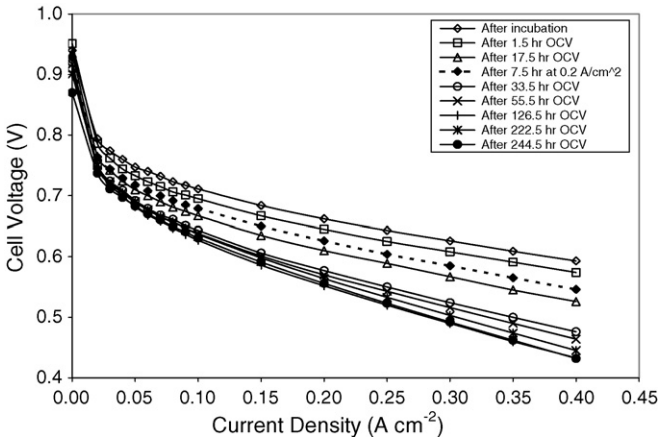

Fig. 3. Polarization curves after different number of hours at open circuit voltage (all solid lines). The dashed line shows the polarization curve after operating the cell at 0.2 A cm^{-2} for 7.5 h following a previous 17.5 h of open circuit voltage.

or so. Afterwards, the decline became much slower. Therefore, the experiment was stopped after a total of 350 h of testing.

The polarization curves at 1.35 times air stoichiometric after different hours of OCV are shown in Fig. 3. The hours shown in the legend are accumulated number of hours at OCV. Clearly, the performance loss occurred throughout the entire current density region, and most of the loss occurred in the first 33.5 h. Afterwards, the performance decline rate slowed down significantly.

The dashed line shown in Fig. 3 is the polarization curve after the fuel cell was set at 0.2 A cm^{-2} for 7.5 h following 17.5 h of OCV. The entire polarization curve became higher than that after 17.5 h of OCV. However, when the fuel cell was set at OCV again, the polarization curve decreased faster, giving up all the gain achieved from running at 0.2 A cm^{-2}, similar to that observed in Figs. 1 and 2.

During the OCV testing process, electrochemical impedance spectra were taken periodically in order to monitor the changes of the cathode kinetic activity and the mass transport resistance. Fig. 4a shows the EIS obtained at a fuel cell current density of 0.2 A cm^{-2} with 1.35 times stoichiometric air flow after 1.5 and 244.5 h of OCV, respectively. Both spectra show two distinct arcs in the high and low frequency regions, representing the electrode activation resistance and the mass transport resistance, respectively. Clearly, both the activation resistance and the mass transport resistance increased significantly after 244.5 h of OCV.

Fig. 4b shows the EIS with 4.0 times air stoichiometry. Although there are still two arcs in high and low frequency regions, the arcs at the lower frequency region almost disappeared. This indicated that the fuel cell performance loss due to mass transport resistance were insignificant when the air stoichiometry was as high as 4.0. Meanwhile, the arc in the high frequency region was significantly larger after 244.5 h of OCV than that after 1.5 h of OCV, pointing to the loss of catalyst activity that was observed with the results obtained at 1.35 times air stoichiometry (Fig. 4a).

The (projected) intercepts of the lowest frequency at the real impedance axis after 244.5 h of OCV were about 1.16 (Fig. 4a) and 0.69 Ω cm^2 (Fig. 4b) at 1.35 and 4.0 air stoichiometry, respectively. If we assume that the activation resistance was

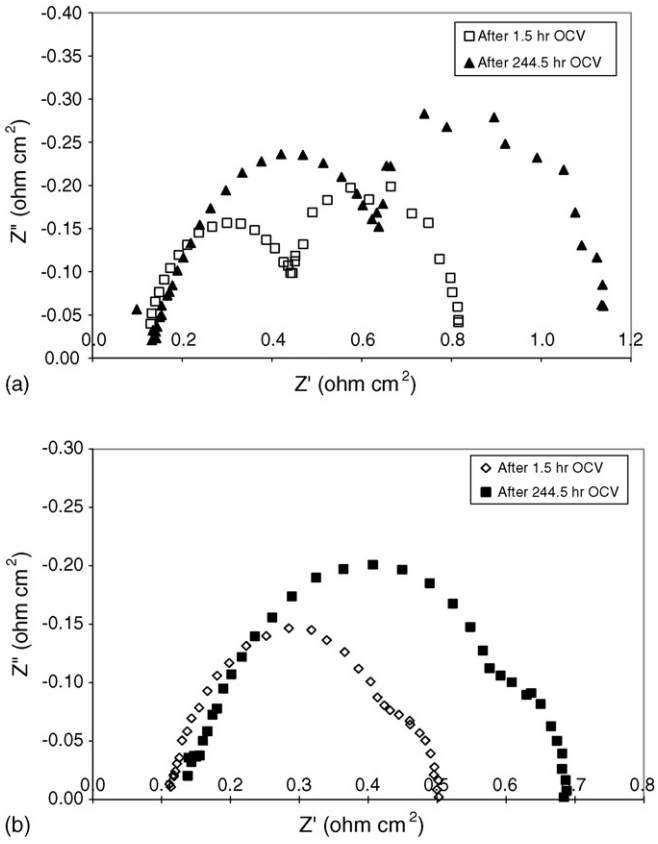

Fig. 4. EIS after 1.5 and 244.5 h of open circuit voltage with 1.35 (a) and 4.0 (b) air stoichiometry, respectively.

not significantly affected by the air stoichiometry change, the difference between the two intercepts, which was 0.47 Ω cm^2 (1.16–0.69), represented the difference in mass transport resistance between at 1.35 and 4.0 times air stoichiometry. Referring to Fig. 2, the difference in cell voltage at 0.2 A cm^{-2} between 1.35 and 4.0 times stoichiometry after 244.5 h of OCV tests was 35 mV (0.567–0.532 V). So, it can be roughly estimated that a difference of 0.47 Ω cm^2 in mass transport resistance led to 35 mV cell voltage drop at a current density of 0.2 A cm^{-2}. However, multiplying 0.47 Ω cm^2 with the current density of 0.2 A cm^{-2} results in 94 mV, which is much larger than the measured 35 mV loss. So, the mass transport resistance obtained from EIS cannot be directly translated into cell voltage drop by multiplying it with the current density. In this case, the result from the simple multiplication was nearly as three times large as the actual cell voltage drop due to the mass transport resistance.

The intercepts at the real axis at the highest frequency were about 0.13 Ω cm^2 from both Fig. 4a and 4b. This resistance represents the total resistance of the membrane (ionic) and the contact resistance among cell components (electronic) (e.g., between gas diffusion media and current collecting plates). This total resistance did not show any apparent change after 244.5 h of OCV tests.

Referring to Fig. 3, it may be seen that the performance drop is essentially linear within the current density of 0.15–0.4 A cm^{-2} for all the polarization curves. The slopes, calculated by $\Delta V/\Delta I$, ranged from 0.39 to 0.66 Ω cm^2, for the polarization curves after

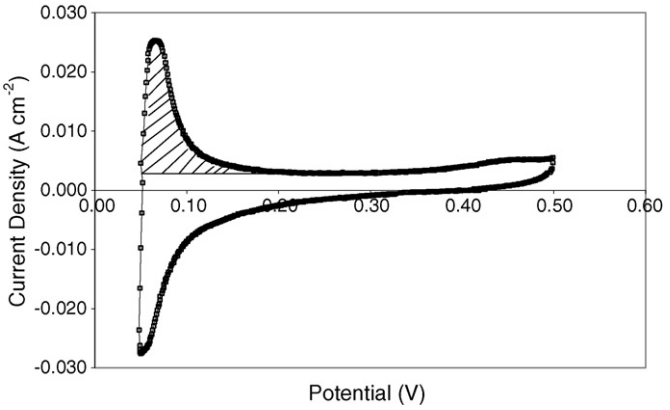

Fig. 5. Cathode cyclic voltammogram of the MEA tested at OCV for 244.5 h. Potential scan rate 20 mV s^{-1}.

incubation and after 244.5 h of OCV test, respectively. Since the total resistance did not change based on results from Fig. 4, the increase in the slope according to the above calculation ($0.27 = 0.66 - 0.39\ \Omega\,cm^2$) was due to both increased catalyst activity loss and increased mass transport resistance. This has several implications. First, using the slope of the linear region of a polarization curve to estimate the total resistance (contact plus ionic) will lead to an exaggerated result. Second, although the linear decline of a polarization curve fits Ohm's Law well (i.e., IR drop), it actually also includes losses due to the mass transport resistance and the activation overpotentials.

Hydrogen desorption peak area was used to estimate the electrochemical active surface area of the cathode. Fig. 5 shows the cathode cyclic voltammogram of the MEA after 244.5 h of tests at OCV. At 180 °C, only one pair of adsorption and desorption peaks were observed, in contrast to lower temperature PEM fuel cells where two pairs of adsorption and desorption peaks are normally observed. The lower potential limit for the cathodic scan (higher to lower potential scan) is always difficult to determine for low catalyst-loaded electrodes, which surely introduces more errors to the real peak areas that are related to hydrogen adsorption and desorption instead of hydrogen evolution. We determined the lower potential limits by trial and error, and only intended to make relative comparisons. The integrated charge under the hydrogen desorption peak (shaded area) was about 2.1 C (per 45 cm^2), which was 38% less than that of a fresh MEA that normally has a charge of 3.4 C. So, significant electrochemical active surface area loss occurred to the tested MEA.

X-ray diffraction was used to estimate the catalyst particle crystallite size changes at both the cathode and the anode. The electrodes were peeled off of the membrane and cut to a size of about 1 cm^2, and the anode and the cathode were measured separately. Three Pt peaks were observed at 39.8° (1 1 1, crystalline facet), 46.2° (2 0 0), and 67.6° (2 2 0). These peaks were all much sharper for the tested cathode than the fresh cathode, indicating that the Pt crystallite size increased in the tested cathode. Using the Debye–Scherrer equation:

$$\text{Crystallite size} = \frac{0.9\,\lambda}{\text{FWHM}\cos\theta} \quad (1)$$

Table 1
Normalized cathode Pt crystallite size estimated by XRD measurement

Sample	Pt peak position (degrees = 2θ)	Normalized crystallite size (nm)
Fresh cathode	39.9° (1 1 1)	1.6
	46.1° (2 0 0)	1.0
	67.7° (2 2 0)	3.2
Tested cathode	39.8° (1 1 1)	5.6
	46.2° (2 0 0)	5.3
	67.7° (2 2 0)	7.7

where λ, FWHM, and θ are the X-ray wavelength, full width at half maximum of the peak, and X-ray beam incidence angle, respectively, the Pt crystallite sizes were estimated. Table 1 shows the results that are normalized by taking the smallest crystallite size as 1.0. The Pt crystallite size increased by as much as 430% after 244.5 h of testing at OCV.

For the anodes, the three Pt peaks did not show significant difference between the fresh and tested MEAs. The estimated Pt crystallite sizes were almost the same for the fresh and tested anodes. Table 2 shows the normalized particle crystallite size by taking the smallest one as 1.0. Obviously, the low potential (∼0 V) and the absence of water either as liquid or vapor at the anode provide a favorable condition for Pt crystallites not to grow.

It is believed that the cathode Pt crystallite size increase resulting from operation at OCV is a major cause of permanent OCV decline and fuel cell performance loss. Several factors are likely to contribute to the quick growth of Pt particles. First, the high temperature (e.g., 180 °C) and potential (e.g., OCV) could elevate Pt dissolution and re-deposition rates ([17] and references therein). Since the anode catalyst crystallite size showed almost no change, it demonstrated that potential has much higher impact than temperature on the growth of the crystallites. Pt particles should also have higher mobility at higher temperatures, so their agglomeration rate will be greater. Second, the high temperature and potential could lead to a high corrosion rate of the carbon catalyst support. Carbon corrosion could weaken or even sever the attachment of Pt particles to the support, thus accelerating the Pt agglomeration rate as well ([13] and references therein). Stabilizing the Pt particles by using Pt alloys [23–25] and stabilizing the support by using graphitic carbon [26] should slow down the growth of the Pt particles. Creating some physical barriers against the movement of catalyst particles could also be

Table 2
Normalized anode Pt crystallite size estimated by XRD measurement

Sample	Pt peak position (degrees = 2θ)	Normalized crystallite size (nm)
Fresh anode	39.8° (1 1 1)	1.4
	46.1° (2 0 0)	1.0
	67.5° (2 2 0)	2.4
Tested anode	39.8° (1 1 1)	1.7
	46.2° (2 0 0)	1.0
	67.7° (2 2 0)	2.3

effective in reducing the growth of the particles. For example, Kunz invented a method by depositing catalyst particles in pits or dents that were purposely created on the surface of a carbon support using a metal oxidizing agent before the fuel cell catalyst deposition step [26]. The pits hindered the movement of the fuel cell catalysts and thus reduced their growth rate. Jalan and Bushnell invented a method of depositing porous carbon around the supported catalyst particles to reduce the movement and thus the growth of the particles [27].

Another major factor responsible for the performance loss is the mass transport resistance increase as illustrated by the EIS results shown in Fig. 4. The mass transport resistance increase is most likely due to the surface oxidation of the carbon catalyst support. The oxidation makes the surface of the support more hydrophilic and thus it is more readily to be flooded by the phosphoric acid. Although the carbon materials in the electrode backing layer could also make some contributions to the increased mass transport resistance, the impact is expected to be minor due to the absence of catalysts in the backing layer to catalyze carbon oxidation.

It is speculated that the initial OCV increase in the first 37 min (Fig. 1) is likely to be due to the following two reasons. First, it could be due to the oxidation of the carbon catalyst-support surface that caused the surface to be better wetted by phosphoric acid when inadequate wetting of the catalyst support existed in the very beginning of the fuel cell testing. Second, it could be due to catalyst surface cleaning through an oxidation mechanism to remove potentially existing adsorbents.

The discrepancy between the cathode electrochemical active surface area loss (38%) and the cathode catalyst crystallite size increase (2.4–5.3 times) can be attributed to several reasons. First, XRD measures the crystallite size rather than the particle size and a particle could contain many smaller crystallites. In contrast, the electrochemical active surface area estimated by cyclic voltammetry reflects the particle size rather than the crystallite size. So, the two measurements are not supposed to give the same results. Second, XRD determines the volume averaged crystallite size, and it may undercount the smaller crystallites. This kind of discrepancy was observed by Ferreira et al for PEM fuel cells as well [17]. In addition, for the three types of crystallites measured here, their relative distributions were not determined.

It is clear from this investigation that a PBI–H_3PO_4 fuel cell system should be operated in such a way that the open circuit voltage and the time at OCV are minimized or completely avoided. This conclusion is in agreement wth previous studies on both PAFCs and PEMFCs [1–3,13,17]. Several methods could be used to achieve this goal. First, the fuel cell should be operated continuously whenever possible. When there is no load demand, the fuel cell could be used to power some parasitic load, and this additional load could be the fuel cell system itself (including parasitic power requirements) to keep the fuel cell warm. Keeping the fuel cell warm also enables faster restart of the fuel cell system, and minimizes potential freezing of the liquid electrolyte. Repeated freeze–thaw cycling of the electrolyte could seriously damage the fuel cell due to the stress created by the volume change.

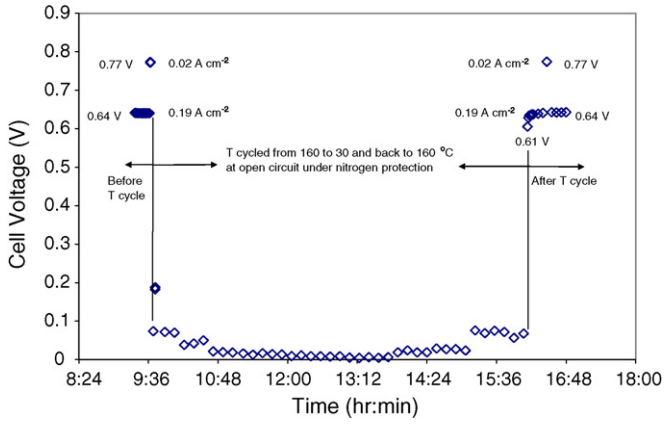

Fig. 6. Effect of cycling cell temperature between 160 and 30 °C on fuel cell performance. 160 °C cell temperature and 1.2/1.35 hydrogen/air stoichiometry when the fuel cell was loaded with 0.02 and 0.19 A cm^{-2} current densities; nitrogen flowed in the cathode and a resistor was used to connect the anode and cathode during the temperature cycling period at open circuit.

Second, if a shut down is unavoidable, the air in the cathode should be completely consumed before the fuel cell is shut down. This can be done by using a resistive load [28–30] or by purging the cathode of the fuel cell with an inert gas such as nitrogen and carbon dioxide immediately after shutdown. Without air in the cathode, the cell potential will be far less than the normal OCV even at open circuit.

The effectiveness of the last two methods was demonstrated by the following experiments. Fig. 6 shows an experiment with the cell temperature cycled from 160 to 30 C and back to 160 C in about 6.5 h. When the cycling was started, a resistor of 1 Ω was used to connect the anode and cathode before the last load, which was 0.02 A cm^{-2}, was disconnected. Immediately after the load was removed, nitrogen was supplied to the cathode to displace air, and the nitrogen flow was continued during the 6.5 h temperature cycling process. The OCV of the cell was nearly 0 V during this time. When the cell temperature returned to about 150 °C, air was reintroduced into the cathode, and a load of 0.19 A cm^{-2} was applied. The cell voltage was slightly lower in the beginning (0.61 V versus 0.64 V), but once the temperature reached 160 °C, the cell voltage became the same as that before the temperature cycling started. Also, the cell voltage at 0.02 A cm^{-2} was the same before and after the temperature cycling (0.77 V). Therefore, although the cell was exposed to open circuit for 6.5 h, it did not lose any performance due to controlling the OCV to about 0 V through the use of a load resistor and an inert gas.

An example of an unavoidable interruption in fuel cell operation during endurance testing is periodic characterization by various techniques in order to gain information about the cell at different stages of the endurance test. One common characterization technique is the electrochemical impedance spectroscopy. Such a measurement gives information about the changes in resistance, catalyst activity, and electrode mass transport resistance. However, if the cell was not controlled properly, the exposure to OCV will cause degradation of the cell. The performance loss may be mistakenly attributed to the interruption of EIS itself. Fig. 7 shows the performance of a fuel cell before

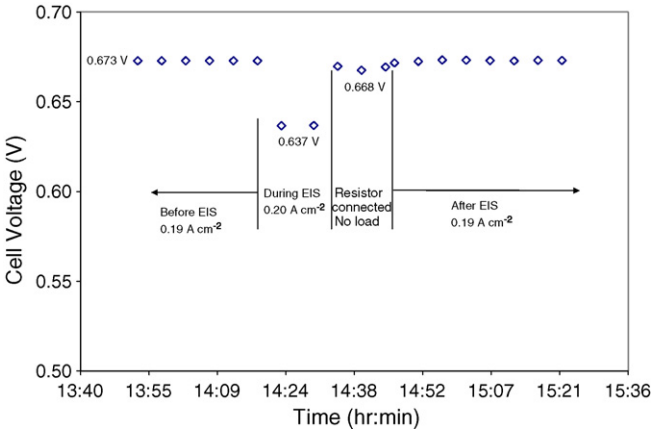

Fig. 7. Effect of performing electrochemical impedance spectroscopy on fuel cell performance. 160 °C cell temperature and 1.2/1.35 hydrogen/air stoichiometry when the fuel cell was loaded with 0.19 A cm^{-2} current density.

and after a 30 min interruption to perform an EIS measurement. Before the cell was interrupted for the connection of the impedance analyzer, an adjustable resistor was used to connect the anode and cathode so that the cell did not expose to OCV. After the impedance analyzer was connected to the cell and readied for the measurement, a current density of 0.19 A cm^{-2} was applied to the cell by the impedance analyzer, and the resistor was then disconnected. The EIS measurement was completed in 15 min, and the resistor was reconnected to the cell again before the impedance analyzer was disconnected from the cell. Another 15 min elapsed before a load of 0.19 A cm^{-2} was applied to the cell again. During the entire 30 min interruption period, air flow was maintained through the cathode but the cell voltage was controlled at a value (0.668 V) less than that (0.673 V) at a load of 0.19 A cm^{-2} by the adjustable resistor. No performance loss was observed after the interruption.

4. Conclusions

It has been shown that allowing a PBI–H_3PO_4 high temperature fuel cell to operate at OCV has a significantly negative impact on OCV and the fuel cell performance. The decline was exponential and most of the loss occurred in the first 50 h of exposure to OCV. Both the cathode activation resistance and the mass transport resistance increased significantly in this process. After 244.5 h of OCV tests, the cathode Pt crystallite size increased to as much as 5.3 times of its original value, while the anode Pt crystallite size showed little change. Extended operation at OCV should be avoided to prolong the life of the high temperature cells.

Acknowledgments

This research was supported in part by the U.S. Department of Energy, Contract No. DE-FC36-03GO13101. Many thanks to colleagues at Albany NanoTech for their assistance in performing the XRD analyses. The authors are grateful to Dr. Thomas Schmidt of PEMEAS GmbH and Ms. Cynthia Mahoney White, Ms. Rhonda Staudt, Mr. Daniel Beaty, and Mr. Jeffrey Boyer of Plug Power for their critical review.

References

[1] R.D. Breault, Stack materials and stack design, in: W. Vielstich, A. Lamm, H.A. Gasteiger (Eds.), Handbook of Fuel Cells—Fundamentals Technology and Applications, vol. 4, John Wiley & Sons, 2003, pp. 797–810.
[2] D.A. Landsman, F.J. Luczak, Catalyst studies and coating technologies, in: W. Vielstich, A. Lamm, H.A. Gasteiger (Eds.), Handbook of Fuel Cells—Fundamentals Technology and Applications, vol. 4, John Wiley & Sons, 2003, pp. 811–831.
[3] J.M. King, B. McDonald, Experience with 200 kW PC25 fuel cell power plant, in: W. Vielstich, A. Lamm, H.A. Gasteiger (Eds.), Handbook of Fuel Cells—Fundamentals Technology and Applications, vol. 4, John Wiley & Sons, 2003, pp. 832–843.
[4] R.D. Breault, US Patent No. 4,017,664 (1997).
[5] J.S. Wainright, J.T. Wang, R.F. Savinell, M.H. Litt, J. Electrochem. Soc. 142 (1995) L121.
[6] D. Weng, J.S. Wainright, U. Landau, R.F. Savinell, J. Electrochem. Soc. 143 (1996) 1260.
[7] S.R. Samms, S. Wasmus, R.R. Savinell, J. Electrochem. Soc. 143 (1996) 1225.
[8] J.T. Wang, J.S. Wainright, R.F. Savinell, M.H. Litt, J. Appl. Electrochem. 26 (1996) 751.
[9] J.J. Fontanella, M.C. Wintersgill, J.S. Wainright, R.F. Savinell, M.H. Litt, Electrochim. Acta 43 (1998) 1289.
[10] Y.L. Ma, J.S. Wainright, M.H. Litt, R.F. Savinell, J. Electrochem. Soc. 151 (2004) A8.
[11] L. Xiao, H. Zhang, E. Scanlon, L.S. Ramanathan, E.-W. Choe, D. Rogers, T. Apple, B.C. Benicewicz, Chem. Mater. 17 (2005) 5328.
[12] L. Xiao, H. Zhang, J. Jana, E. Scanlon, R. Chen, E.-W. Choe, L.S. Ramanathan, S. Yu, B.C. Benicewicz, Fuel Cells 5 (2005) 287.
[13] M.F. Mathias, R. Makharia, H.A. Gasteiger, J.J. Conley, T.J. Fuller, C.J. Gittleman, S.S. Kocha, D.P. Miller, C.K. Mittelsteadt, T. Xie, S.G. Yan, P.T. Yu, Interface 14 (2005) 24.
[14] K. Kinoshita, Carbon—Electrochemical and Physicochemical Properties, John Wiley & Sons, 1988.
[15] J. Xie, D.L. Wood III, D.M. Wayne, T.A. Zawodzinski, P. Atanassov, R.L. Borup, J. Electrochem. Soc. 152 (2005) A104.
[16] T. Kinumoto, K. Takai, Y. Iriyama, T. Abe, M. Inaba, Z. Ogumi, J. Electrochem. Soc. 153 (2006) A58.
[17] R.J. Ferreira, G.J. La O', Y. Shao-Horn, D. Morgan, R. Makharia, S. Kocha, H.A. Gasteiger, J. Electrochem. Soc. 152 (2005) A2256.
[18] R.M. Darling, J.P. Meyers, J. Electrochem. Soc. 152 (2005) A242.
[19] P. Yu, M. Pemberton, P. Plasse, J. Power Sources 144 (2005) 11.
[20] J. Aragane, H. Urushibata, T. Murahashi, J. Appl. Electrochem. 26 (1996) 147.
[21] J. Aragane, T. Murahashi, T. Odaka, J. Electrochem. Soc. 135 (1988) 844.
[22] P. Bindra, S.J. Clouser, E. Yeager, J. Electrochem. Soc. 126 (1979) 1631.
[23] F.J. Luczak, D.A. Landsman, US Patent No. 4,613,582 (1986).
[24] F.J. Luczak, D.A. Landsman, US Patent No. 4,677,092 (1987).
[25] V.M. Jalan, US Patent No. 5,079,107 (1992).
[26] H.R. Kunz, US Patent No. 4,028,274 (1977).
[27] V.M. Jalan, C. L. Bushnell, US Patent No. 4,137,372 (1979).
[28] L.L. Van Dine, M.M. Steinbugler, C.A. Reiser, G.W. Scheffler, US Patent No. 6,514,635 (2003).
[29] R.J. Balliet, C.A. Reiser, US Patent No. 6,835,479 (2004).
[30] T.A. Bekkedahl, L.J. Bregoli, R.D. Breault, E.A. Dykeman, J.P. Meyers, T.W. Patterson, T. Skiba, C. Vargas, D. Yang, J.S. Yi, US Patent No. 6,913,845 (2005).